Magnetic Resonance in Medicine 51:577–585 (2004)

Fast, Pseudo-Continuous Arterial Spin Labeling for Functional Imaging Using a Two-Coil System

Luis Hernandez-Garcia,[1,2*] Gregory R. Lee,[1,2] Alberto L. Vazquez,[1,2] and Douglas C. Noll[1,2]

A fast, two-coil, pseudo-continuous labeling scheme is presented. This new scheme permits the collection of a multislice subtraction pair in <3 s, depending on the subject's arterial transit times. The method consists of acquiring both control and tag images immediately after a labeling period that matches the arterial transit time. The theoretical basis of the technique, and simulations of the signal during changes in both transit time and perfusion are presented. Experimental data from functional imaging experiments were collected to demonstrate the technique and its characteristics. Magn Reson Med 51:577–585, 2004. © 2004 Wiley-Liss, Inc.

Blood oxygenation level-dependent (BOLD) contrast functional MRI (fMRI) is currently the dominant technique for functional imaging, and it has produced a wealth of information about the brain's cognitive function. Although BOLD techniques offer great detection power, they also have limitations; therefore, there is strong interest in the development of perfusion-based functional imaging techniques. These limitations include the complexity of the mechanism that gives rise to the BOLD signal (1,2), the nonlinearity of that signal (3,4), the temporal noise characteristics (5), and the well-known sensitivity to susceptibility artifacts.

In contrast, perfusion is a quantifiable physiological parameter that is easier to relate to neuronal metabolism. Furthermore, our ability to dynamically measure cerebral blood flow (CBF) is crucial for understanding the BOLD effect. Recent animal studies conducted at high field and high spatial resolution indicated that CBF changes are more localized to the parenchyma than the BOLD effect, consistent with the notion that the BOLD effect is weighted toward draining veins (6,7).

In the light of these considerations, it is not surprising that there has been extensive work toward the development of rapid, noninvasive cerebral perfusion measurement techniques over the last decade. Among these, arterial spin labeling (ASL) (8–11), which employs magnetically labeled arterial water as an endogenous tracer, is the most promising. One additional advantage of ASL techniques is the nature of the noise present along the temporal dimension. fMRI time series data contain severe low-frequency, auto-correlated drifts, the amplitude of which is much larger than the BOLD signal itself (12). These low-frequency drifts are not present in ASL time series, which effectively enables the use of very low-frequency functional paradigms (13). Furthermore, Desmond and Glover (14) recently showed that the power of an fMRI study is largely determined by the intersubject variance of the activation response intensity. In a BOLD experiment, this variance stems from both physiological and hardware variability, whereas in an ASL experiment, the variability observed is mostly due to physiological sources, since the hardware effects are largely subtracted out.

ASL techniques also present a number of challenges. These techniques suffer from low SNR, since <10% of the water in a given voxel is contributed by blood (15,16), and the label decays at a quick rate. This problem can be partially alleviated by increasing the amount of label that is introduced into the tissue, by using longer RF labeling pulses until the tissue of interest becomes saturated with labeled blood. This approach is referred to as continuous ASL (CASL). Another major limitation of ASL techniques, particularly CASL, is low temporal resolution (and consequently the SNR because of a lower number of averages in a given time period). This is because the acquisition of ASL image pairs usually takes 3–8 s, depending on the amount of time it takes to label the arterial blood. Collecting multislice data can also be challenging because the imaging RF pulses can interfere with the inversion label of the arterial water (17,18). In addition, one must acquire all slices within a short period of time in order to sample the label before it clears from the tissue of interest.

Wong et al. (19) proposed a pulsed labeling scheme in which the control image is acquired immediately after labeling, before the spins reach the tissue of interest. Thus the tagged image is acquired after the control period, when the inversion tag reaches the tissue of interest. The net effect of this approach, dubbed "turbo-ASL," is a marked increase in the temporal resolution of the measurement.

We have found that by choosing the right tagging duration and TR, one can take advantage of the wash-in and wash-out kinetics of the system to dramatically reduce the time it takes to collect a CASL image pair. This is similar to the turbo-ASL approach.

In traditional CASL experiments, an inversion label is applied until a steady-state concentration of the label is built up in the tissue of interest. Subsequently, a second reference (control) image is collected by allowing all of the label to clear the tissue. However, in the approach presented here, we propose to speed up the measurement by collecting the control and labeled images after a single labeling period. In other words, we apply the label only until its leading edge is about to reach the imaging slice,

[1]fMRI Laboratory, University of Michigan, Ann Arbor, Michigan.

[2]Department of Biomedical Engineering, University of Michigan, Ann Arbor, Michigan.

Grant sponsors: University of Michigan (fMRI Laboratory and Center for Biomedical Engineering Research); Raynor Foundation.

*Correspondence to: Luis Hernandez-Garcia, Ph.D., fMRI Laboratory, University of Michigan, 2360 Bonisteel Ave., Ann Arbor, MI 48109-2108. E-mail: hernan@umich.edu

Received 17 June 2003; revised 21 October 2003; accepted 21 October 2003.

DOI 10.1002/mrm.10733

Published online in Wiley InterScience (www.interscience.wiley.com).

and then immediately collect the "control" image. The "tag" image is acquired at the following TR after the back edge of the inverted spins have arrived at the imaging plane. By using this pseudo-continuous approach, we give up some of the SNR advantage afforded by CASL and we increase the sensitivity of the ASL signal to arterial transit times, but we are able to increase the temporal resolution of the ASL measurement, and detect and characterize perfusion responses to event-related experiments.

In this work we describe the theoretical framework for this new method (which we term "turbo-CASL"), explore the effect of transit time changes on the technique, and demonstrate its use on both block-design and event-related fMRI data.

MATERIALS AND METHODS

Simulations

The kinetics of a turbo-ASL system, such as the one described by Wong et al. (19), can be described by the same first-order kinetic model proposed by Buxton et al. (20):

$$\Delta M(t) = 2\alpha f \cdot M_{oA} C(t)^* [r(t)m(t)], \qquad [1]$$

where ΔM is the CASL subtraction signal, α is the degree of inversion of the tagged arterial water, M_{oA} is the arterial blood magnetization, f is the perfusion rate, $c(t)$ describes the arterial input function into the tissue, $r(t)$ is a function describing the wash-out of tag from the tissue, and $m(t)$ is the exponential decay of the tag due to T_1.

We modified this framework to include the effect of sampling the tag at the slice of interest. In practice, the accumulated tag is destroyed each TR when the different slices are excited by the RF pulses of the acquisition sequence, and the model must be revised to account for this effect. If sampling of individual slices is fast enough (<50 ms), the destroyed tag will not have time to affect the adjacent slices. Thus, in our model we "reset" the accumulated tag to zero every time the slice is acquired.

To compute the amount of tag present in the slice when we take this periodic destruction of the tag into consideration, we must divide the experiment time into equal segments of TR duration. The analytical solution to the equation then has two possible cases (depicted in Fig. 1), as described below.

Case 1

The delivery of tag to the imaging slice occurs within a single TR interval. The leading edge of the tagged spins arrive at the imaging slice in the $(N-1)$th TR interval and the trailing edge arrives before N * TR. In this case, the solution is given by:

$$\Delta M(t) = \begin{cases} 0 & 0 < t < \Delta t \\ C_1^*(1 - e^{-(t-\Delta t)/T1eff}) & \Delta t < t < \Delta t + \tau \\ C_1^* e^{-t}/T1eff(e^{(\Delta t + \tau)/T1eff} - e^{\Delta t/T1eff}) & \Delta t + \tau < t < nTR \\ 0 & t > nTR \end{cases}. \qquad [2]$$

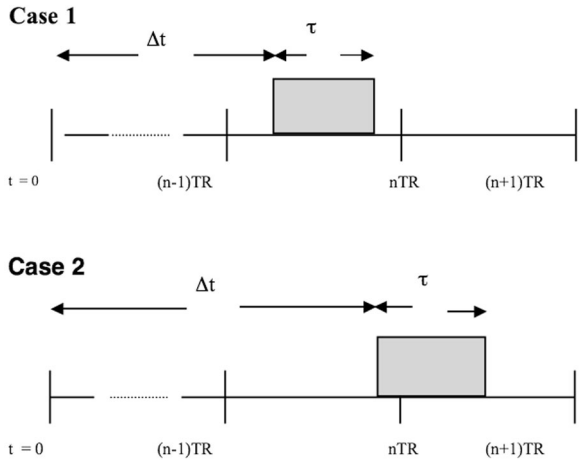

FIG. 1. The two possible cases for arrival of the tag. It is assumed that labeling begins at t = 0, and the tag arrives at the imaging slice during the shaded block of time (N = 2 for turbo-CASL).

Case 2

The delivery of tag to the imaging slice occurs over two TR intervals. The leading edge of the tagged spins arrives during the $(N-1)$st TR interval, and the trailing edge arrives before $(N+1)$*TR. Here the solution is:

$$\Delta M(t) = \begin{cases} 0 & 0 < t < \Delta t \\ C_1^*(1 - e^{-(t-\Delta t)/T1eff}) & \Delta t < t < nTR \\ C_1^*(1 - e^{-(t-nTR)/T1eff}) & nTR < t < \Delta t + \tau \\ C_1^* e^{-t/T1eff}(e^{(\Delta t+\tau)/T1eff} - e^{nTR/T1eff}) & \Delta t + \tau < t < (n+1)TR \\ 0 & t > (n+1)TR \end{cases}, \qquad [3]$$

Where

$$C_1 = 2\alpha M_{0A} f^* T1_{eff}^* e^{-\Delta t/T1arterial}, \qquad [4]$$

and

$$\frac{1}{T1_{eff}} = \frac{1}{T1_{tissue}} + \frac{f}{\lambda}, \qquad [5]$$

In the above equations, Δt is the arterial transit time, τ is the duration of the labeling RF, and 1 is the blood–brain partition coefficent. Using this framework, we simulated the behavior of the ASL signal as a function of TR (tagging duration = TR − 200 ms for acquisition of four slices), given specific transit times (1, 1.5, and 2 s) between the labeling and imaging planes.

In a second simulation, the transit time was varied while the sequence parameters were held fixed (TR = 1.5 s, tagging duration = 1.45 s). In both cases, the following constants were used in the model (f = 0.015 ml/g/s, M_{oA} = 3000, $T_{1\text{arterial}}$ = 1.5 s, $T_{1\text{tissue}}$ = 1.6 s, α = 0.9, λ = 0.9 ml/g). f was chosen as a typical (9,21) gray-matter perfusion measurement (90 ml/min/100 g), M_{oA} is an arbitrary signal intensity, T_1 for tissue was estimated from

earlier measurements of gray matter at our laboratory, α was arbitrarily assumed to be 90% efficient, and $T_{1\text{arterial}}$ and λ were obtained from the literature (22,23). We used the results of these simulations to determine the optimum labeling time for a given transit time, and the effects of errors in the transit time measurement on the measured perfusion signal.

Pulse Sequence Design and Hardware

Imaging was carried out at 3T on a GE (Milwaukee, WI) Signa LX system. ASL was accomplished by the use of a separate transmitter coil placed on the subject's neck, as in previous studies (17,18,24), while imaging was carried out using the standard GE birdcage coil. The labeling coil was a custom figure-eight coil (diameter = 6 cm), built such that the two loops were at a 130° angle relative to each other. The angle between the two loops permitted a better fit of the subjects' neck and greater proximity of the arteries to the focal point of the coil. The labeling coil was powered by a separate signal generator (PTS 500; Programmed Test Sources Inc., Littleton, MD) and amplifier (custom-built by Henry Radio Supply, Los Angeles, CA), which was in turn controlled through TTL pulses from the MRI scanner. Inversion of the spins was verified by separate imaging experiments on humans and on a flow phantom (25) for flow velocities of 20 cm/s. No significant RF bleed-through or coupling between the tagging and imaging coils was found, and no decoupling hardware was necessary.

For the perfusion imaging experiments, four slices were collected with the birdcage coil using a spin-echo spiral sequence (TE = 12 ms, variable TR, flip angle = 90°). In the turbo-CASL experiments, the TR was set to the measured transit time (as described below) between the labeling plane and the volume of interest. The tagging segment consisted of a continuous RF pulse applied with the figure-eight coil described above for a period equal to TR − 230 ms to allow for image acquisition. Tagging was applied on alternating acquisitions.

The protocol described below was carried out on human volunteers ($N = 6$), who were scanned in accordance with the University of Michigan's Internal Review Board regulations.

Arterial Transit Time Measurement During Steady State (Resting and Active)

We collected multislice maps of the arterial transit time from the inversion plane at the neck to the imaging plane during both rest and activation conditions. Transit times were estimated by varying the TR (500, 750, 1000, 1200, 1400, 1600, 1800, 2000, 2400, 3000, and 4000 ms) and keeping the tagging time 230 ms shorter than TR to allow the acquisition of four slices using a forward spiral acquisition (TE = 12 ms, alpha = 90%, and no arterial flow crushers). Under the assumption that flow remained at a steady state during each condition, the data were then fit to the linear Buxton model (Eqs. [3]–[5]) modified for partial saturation of the tag by the imaging pulses using a least-squares fitting routine in Matlab (The Mathworks, South Natick, MA) for each voxel in the image. BOLD contributions to the signal were assumed to be negligible at our choice of TE, and were expected to cancel out in the subtractions.

Transit time maps were collected in this manner during conditions of both rest (the subject lay in the scanner while looking at cross-hairs on a black background) and activation (the subject performed self-paced finger-tapping continuously over the acquisition). For averaging purposes, 16 control/tag pairs were acquired (only eight averages were collected for the 4000-ms case). The total duration of this portion of the experiment was about 10 min. Still under the assumption that flow remained at a steady state during each condition, we were then able to determine the transit time change for the activating voxels (as determined by the "standard" CASL block-design task described below).

A T_1 map was acquired separately by an inversion recovery scheme consisting of the same spiral acquisition used for the ASL images preceded by a hyperbolic secant adiabatic inversion pulse applied TI ms before the acquisition (TR = 10000 ms; TI = 20, 100, 500, 1000, 3000, and 8000 ms). Consequently, the only free parameters in the fit were amplitude and transit time. The fits were carried out using a nonlinear fitting routine in Matlab.

Block-Design Activation Maps

A block-design, bilateral finger-tapping experiment was repeated twice to identify the motor cortex. The activation paradigm consisted of 40 s of rest alternating with 40 s of finger-tapping repeated over five cycles. The subjects received instructions through a visual stimulus presentation screen (IFIS; Psychology Software Tools, Pittsburgh, PA) that displayed the words "REST" and "TAP," and their performance was monitored visually from the control room. The first activation map was collected using a "standard" continuous labeling scheme (TR = 4 s, tag duration = 3 s, post-tagging delay = 0.75 s), and the second one was collected using the turbo-CASL sequence, where the optimal TR was chosen from the transit time mapping experiment above for each individual subject. Typical tagging times and TRs were around 1.2 s and 1.5 s, respectively.

Both control and tagged images were sinc-interpolated separately at every acquisition, which effectively up-sampled the time series by a factor of 2. The resulting tagged-control pairs were subtracted to yield a perfusion-weighted time series of images. Active voxels were identified by correlation to a smoothed boxcar reference function, and time courses were extracted from the active voxels. A significance threshold of $P < 0.002$ was used along with a contiguity threshold that excluded single-voxel activations.

The baseline perfusion signal amplitude was measured for both the standard and turbo techniques by using the mean perfusion image intensity during the "rest" segments of the paradigm. The contrast-to-noise ratio (CNR) was also measured for the average time series over all voxels that were active in both the standard and turbo acquisitions. To compute CNR, this time series was fit to a smoothed boxcar function. The amplitude of the signal increase due to activation was then divided by the square root of the mean square error.

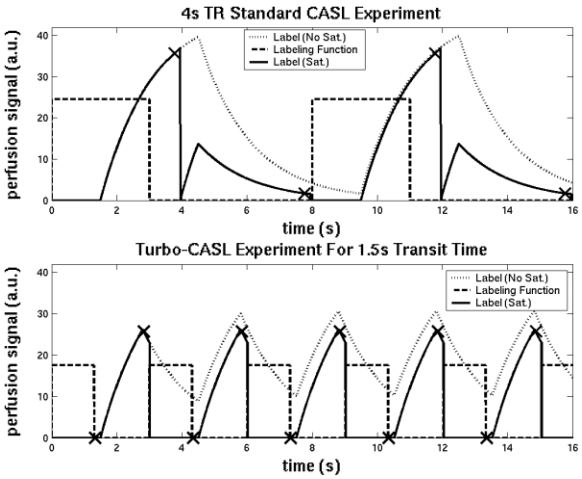

FIG. 2. Simulated signal (top) during a standard CASL experiment, as calculated using Eqs. [2] and [3] (recall that the observed signal is the subtraction of the control image from the tagged image). In this simulation, TR = 4, τ = 3, Δt = 0.75 s, and delay before imaging = 1.5 s. The blue line is the result of the standard model, while the black line takes into account the fact that the tag at the imaging plane is lost after imaging. Each red X indicates a time when image acquisition occurred. Note that the delay between the start of the tagging period and the arrival of the spins at the location of interest is >1 s because of the distance between the location of the inversion coil (neck) and the imaging plane. Our strategy (bottom) consists of collecting the control image before the leading edge of the tag reaches the slice of interest and the tag image after a control period, during which the tag fills the tissue of interest. In this case, TR = 1.5 s, τ =1.3 s, Δt = 1.5 s, and delay before imaging = 4 ms.

Event-Related Activation Experiment

Using the turbo-CASL sequence, we collected a time series of images during a different finger-tapping task consisting of 2 s of tapping followed by 20 s of rest. This paradigm was repeated 30 times, for a total imaging time of 660 s. The data were sinc-interpolated and subtracted, as above, yielding a perfusion-weighted time series. Time courses from the pixels determined to be active in the previous "standard" ASL block-design experiment were extracted and averaged together to form a single time series.

Time Series Processing

After the images were reconstructed, the control and tagged time series were up-sampled through sinc-interpolation such that a control and a tagged image existed at every time point. The images were motion-corrected by applying the rigid-body transformation that minimized the normalized correlation between a standard image and the rest of the time series using the MCFLIRT package (26).

RESULTS

Figure 2 demonstrates the simulated signal behavior for both a standard CASL experiment (top) and a turbo-CASL experiment optimized for a 1.5-s transit time (bottom). In both cases, we show the effect of neglecting the saturation of tag due to the imaging RF. Note how the difference is much more significant in the turbo-CASL approach. The black line is the observed signal when the destruction of the tag by the imaging sequence is taken into account. In practice, the saturation due to a single 90° pulse will be incomplete (according to our previous experience, it may average ~70–80% over the slice). However, the remaining signal that did not get saturated can be safely neglected, as it becomes greatly reduced due to outflow and T_1 decay by the following TR.

The results of the simulation of the signal behavior for a given transit time as a function of TR are shown in Fig. 3 for three different transit times (1, 1.5, and 2 s.). It can be seen that the largest amount of signal is always obtained for very long TR values (>5 s); however, the second highest signal *amplitude* peak occurs at a much shorter TR (i.e., when the TR is equal to the transit time). In the multislice case, the average signal over all four slices still peaks around the point when TR equals the transit time. Note that the signal amplitude of the earlier peaks is reduced somewhat in the multislice case. This is due to the larger portion of the TR that is being used for image acquisition rather than labeling, and underscores the fact that rapid image acquisition is essential to turbo-CASL acquisitions.

Figure 4 shows the effect of a suboptimal choice of TR (i.e., when the transit time is different from that estimated during the optimization of the turbo-CASL sequence). In the figure it can be seen that a transit time of 1 s, for instance, results in no signal appearing in a sequence optimized for a 1.5-s transit time. For some transit times, contrast can even be reversed. From the results of this simulation, it can be seen that a large spread of transit time values within the imaging volume or any substantial shifts in transit time upon activation are undesirable in a turbo-CASL design. The signal amplitude is biased toward a transit time equal to the chosen TR of the sequence.

The appearance of the perfusion images for the various TR values used in the transit time mapping experiment are

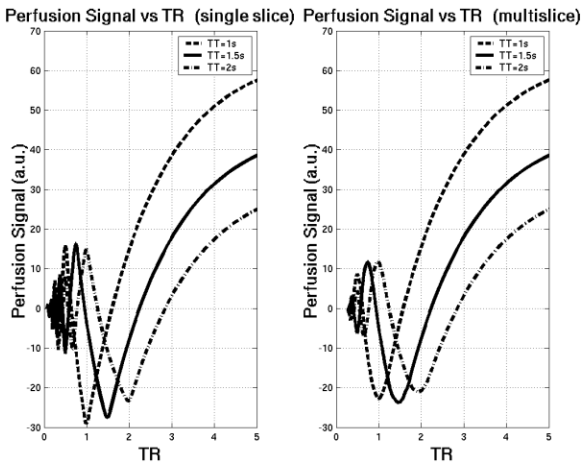

FIG. 3. Accumulated tag as a function of TR in a sequence in which the tagging time is the same as TR minus the time to collect the slices (left). Note that in terms of absolute signal, the second-highest local maximum (minumum in the figure) occurs when TR is approximately the same as the transit time delay. It is also apparent that the perfusion signal in a multislice turbo-CASL sequence is somewhat reduced due to the increased portion of the TR needed for image acquisition (right).

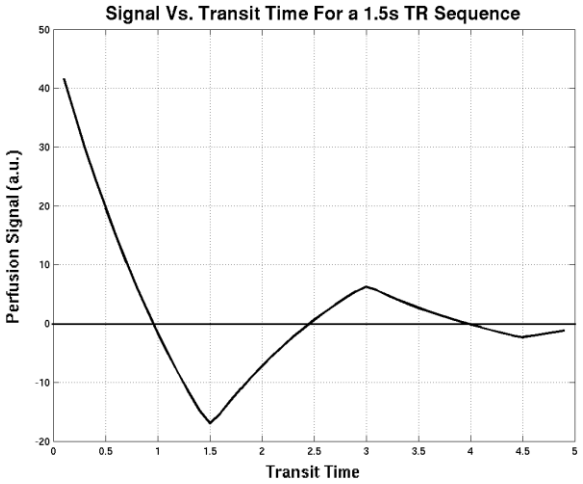

FIG. 4. Observed signal for different transit times when the turbo-CASL sequence is optimized for a 1.5-s transit time (TR = 1.5 s, tag duration = 1.45 s). There is reduced sensitivity for small shifts away from the optimum transit time. In the extreme case, contrast can even be reversed if voxels within the imaging volume have a wide transit-time spread.

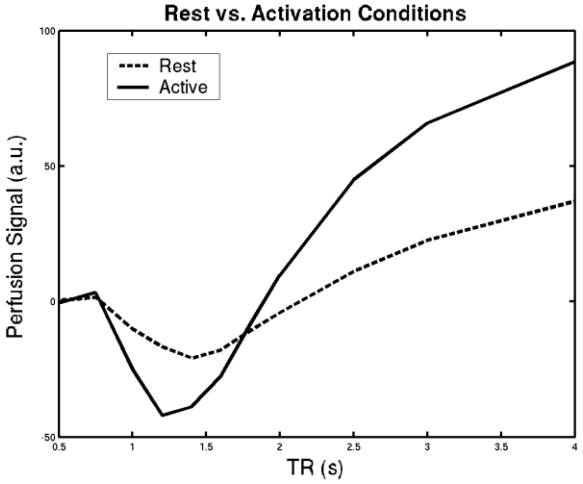

FIG. 6. Measured CASL signals under both rest and activation conditions as a function of TR, averaged over all activating voxels, for subject 1. The negative peaks reveal the arterial transit time under both rest and activation conditions.

shown in Fig. 5. As predicted, there is a local maximum in signal intensity of opposite contrast at a shorter TR value than is traditionally used in CASL experiments.

The measured signal vs. TR for both rest and activation conditions is shown in Fig. 6. These results demonstrate the changes in both perfusion and transit time that occur due to motor activity. The in vivo data reflect the pattern observed in the simulations depicted in Fig. 3. The oscillations of the curve at the low TR values are not apparent in Fig. 6—probably because of the lack of sampling at those time points, or perhaps also because of the "smoothing" effect of a greater distribution of transit times in vivo compared to the simulation (see Fig. 3, right panel). Transit time measurements from human subjects were obtained from fitting plots similar to these for each individual voxel. One subject was excluded from all subsequent analyses due to excessive movement. Note that in addition to fitting the data, the transit time is also evident from the location of the negative peak near 1.5 s. The results from the fits are shown in Table 1. The data indicate that there is a decrease in transit time during the active state relative to the resting state in the motor cortex. In previous experiments (data not shown), we also found that the transit times varied across brain tissue consistently with the anatomy of the cerebral vascular tree (i.e., longer transit times were observed in the occipital regions than in the frontal regions). Focal spots of very short transit times can also be appreciated over the large arteries.

The resulting fits of the model to the measured data under the steady-state rest and activation conditions are shown in Table 1, and a histogram of a representative subject's transit times is shown in Fig. 7. Note that the majority of the transit times fall within a 0.5-s range for this subject. The areas near the midline of the brain in slices 2–4 show the fastest transit time, with most of the longest transit times appearing in the white matter. This pattern of shortest transit times near the midline was consistent over all subjects.

The mean transit times at rest ranged from approximately 1.4–1.7 s in the voxels that showed activation. In the same voxels, the mean shift in transit time was found to be 151 ms ± 44.8 ms (mean ± SD). All of the subjects experienced a >100-ms decrease in transit time in the activating voxels, and a smaller decrease in transit time in the remaining, nonactivating voxels in the brain. This change in transit time was 41.4 ms ± 25.3 ms. We attribute

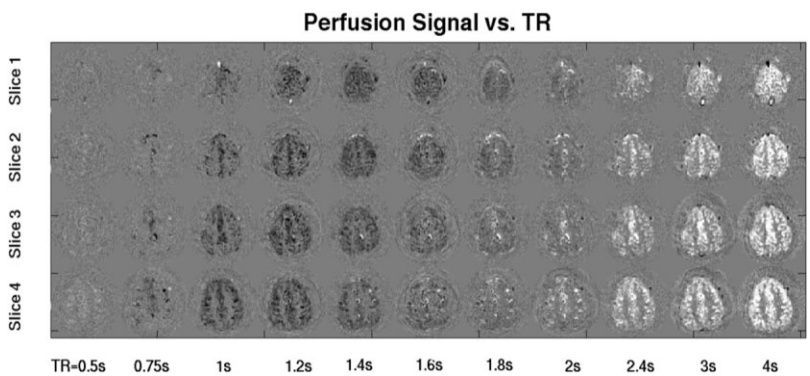

FIG. 5. Perfusion-weighted images for the turbo-CASL sequence with different choices of TR for subject 1 under the resting condition. Note that the images at TRs of 1.2 and 1.4 s are the negative peak predicted by the model. It is readily seen that transit times for large vessels near the midline are the fastest, as these are the first to reverse contrast.

Table 1
Average Transit Time and Signal Amplitude Changes: Active vs. Inactive Voxels

	No. active voxels	Average over active voxels				Average over inactive voxels:	
		Δt: rest (ms)	Δt: active (ms)	Decrease in Δt (ms)	Signal increase (%)	Decrease in Δt (ms)	Signal increase (%)
Subject 1	54	1403	1234	169.7	110.8	53.1	7.41
Subject 2	30	1700	1550	150.7	105.9	43.1	−1.07
Subject 3	29	1746	1634	112.5	66.4	39.0	−0.85
Subject 4	97	1699	1483	216.0	71.7	70.3	26.6
Subject 5	74	1459	1352	106.4	58.1	1.58	11.0
Mean				151.0	82.6	41.4	8.62
SD				44.8	24.1	25.3	11.34

the reduction of transit time in the nonactivated voxels to the contribution from those voxels near the activated area that did not change significantly enough to be classified as active by the statistical map.

The amplitude parameter (C1 in Eqs. [2]–[4]) from the same fits revealed a relative signal increase upon activation (as determined by the magnitude of the scale factor in the transit time fit), which averaged 82.6% ± 24.1%.

The mean baseline perfusion signal over the whole brain for turbo-CASL was reduced by 32.1% ± 12.5% relative to the standard CASL. Our simulations predicted a reduction in signal of only 28.1% and 17.0% for transit times of 1.4 s and 1.6 s, respectively. It is not surprising that the simulations overestimated the signal for turbo-CASL, because they assumed a uniform transit time to all voxels. As noted above, although there is a range of transit times across the brain, the timing of the turbo-CASL scheme can only be optimized for a single transit time.

The average time series over all activating voxels are shown for both the standard and turbo-CASL techniques in Fig. 8. The average CNR obtained using the turbo-CASL method was 3.9, while it was 6.9 using the traditional method (i.e., 42.9% CNR loss in turbo-CASL relative to standard CASL). However, turbo-CASL allowed a greater number of time points (>2.5 times more) to be collected during the same time period, which mitigated the SNR loss by allowing a greater number of averages and thus improved the characterization of the time-series data.

The average perfusion response function across all subjects obtained during the event-related paradigm is shown in Fig. 9. The voxels averaged were those found to be active in the standard CASL block-design experiment.

DISCUSSION

CNR and SNR Issues

It is apparent from the CNR comparison that the turbo-CASL technique suffers from a reduction of CNR as compared to standard CASL. In pulsed turbo-ASL (PASL), very

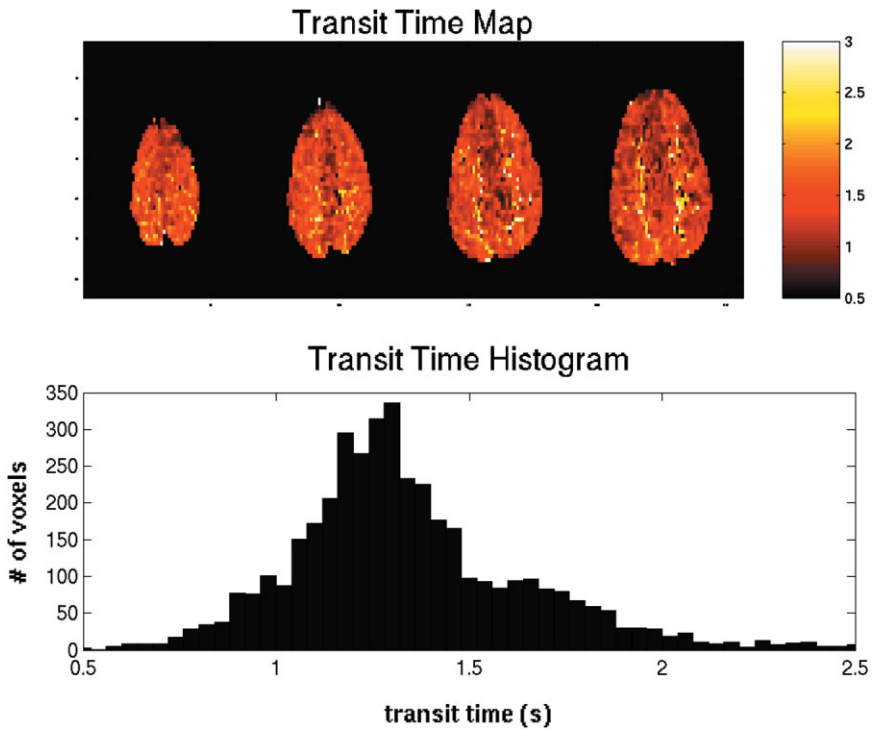

FIG. 7. Map of the transit time (top) and corresponding histogram (bottom) for all four slices through the motor cortex of subject 1. Note that shorter transit times are darker on the display.

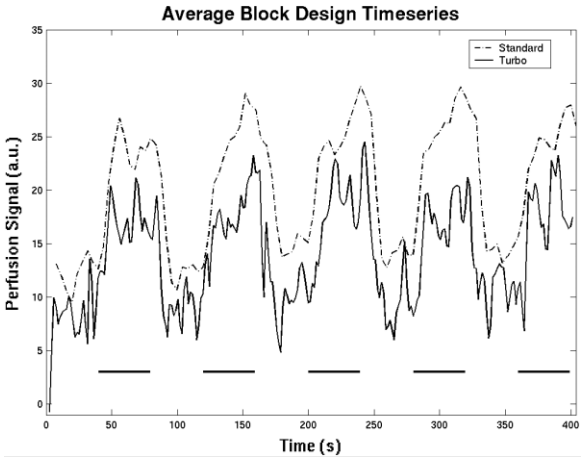

FIG. 8. Averaged time series over all activating voxels for both the standard- and turbo-CASL block-design data (a total of 281 voxels in the standard-CASL case, and 288 voxels in the turbo-CASL case). Note that in practice, the sign of the perfusion signal is opposite in value for these two cases. The absolute value is displayed for easier visual comparison.

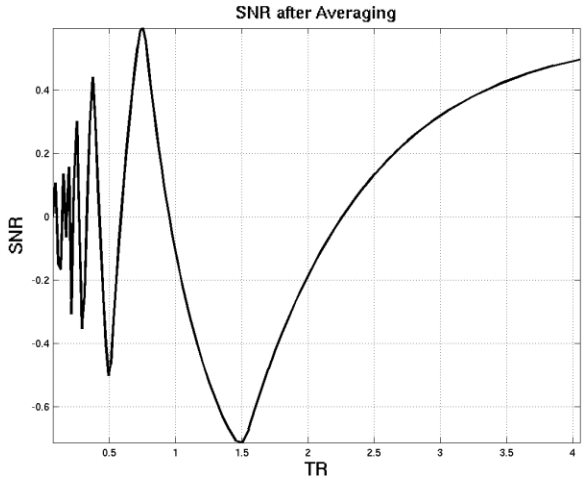

FIG. 10. Estimate of the SNR of an ASL measurement as a function of TR for a fixed experimental period of time in which transit time remains constant at 1.5 s. This estimate was obtained from the calculated amount of tag and the number of averages available during the time period.

little penalty in noise was obtained by going from a 2-s TR to a 1-s TR, because the same duration of tag was used. However, in the CASL implementation, we are not able to use the very long labeling durations that have traditionally given CASL techniques their improved perfusion signal amplitude over PASL techniques. Thus, we lose some of the signal advantage of CASL over PASL by using a turbo implementation of the technique. On the other hand, we are able to collect more data points during the same scanning period, which increases the degrees of freedom available for linear regression (thus recovering some of the sensitivity of the detection), and increases the temporal resolution available to characterize the responses. This is illustrated by the fact that despite the lower CNR of the turbo technique, approximately the same number of significant voxels were found as in the standard case due to the greatly increased degrees of freedom in the statistical analysis (125 or 143 for turbo vs. 50 for standard).

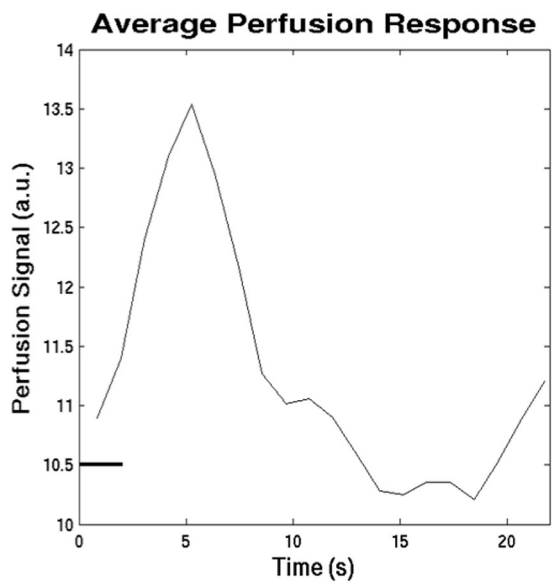

FIG. 9. Averaged perfusion response of the event-related experiment over all activating voxels and all subjects. The active voxels were determined from the standard-CASL block-design experiment.

As regards SNR, the additional number of averages available in the turbo-CASL technique mitigates the SNR loss from the shorter labeling time relative to the standard CASL technique. The number of averages possible within a period of time increases with 1/TR, and consequently the noise can be reduced by the square root of TR. Figure 10 shows an estimate of the SNR of turbo-CASL as a function of TR by dividing the simulated data in Fig. 3 by the square root of TR. Note that in the optimum case (TR = transit time) there is an SNR gain of 40% relative to the continuous case of 4-s labeling.

According to the model, the optimum SNR of the measurement is primarily affected by the choice of TR relative to the transit time. As predicted by Eqs. [2]–[5], the observed signal amplitude will also be affected by the efficiency of the inversion pulses in a linear fashion. The signal amplitude is also affected by the T_1 decay rate of the tissue and the blood in a less straightforward way. The T_1 of the blood affects the scaling in front of the equation, but does not affect the uptake kinetics. The T_1 of the tissue affects the steepness of the uptake of the tag once it reaches the slice. For example, at 1.5T (where the T_1's of blood and tissue are significantly shorter than at 3T), the model predicts 30% less tag, but the optimum tagging time remains the same. The steady state necessary for the standard CASL technique would be achieved slightly earlier at 1.5T than at 3T due to shorter tissue T_1. The optimum tagging time is still determined by the arterial transit time, regardless of the field strength.

Optimizing the Tagging Time

The acquisition scheme consists of applying a tagging pulse and collecting the control image before the tag ar-

rives at the slice of interest, and then collecting the tagged image as the tissue fills with the inversion tag. In this scheme, the tag clears during the application of the next labeling pulse. It is therefore crucial to select the right tagging and sampling times (i.e., by setting the TR to be the same as the transit time between the labeling plane and the imaging plane). Failure to do so can result in severe signal loss and artifactual ASL measurements that do not reflect the changes in flow. In our practical experience with the technique, we have found that we can accurately estimate the resting transit time in <10 min by collecting eight ASL images with tagging times of 800–2000 ms, and TRs set to the tagging time plus an additional 200 ms.

Spatial and Temporal Variability of the Arterial Transit Times

From the simulations, we can see that implemention of the current method hinges on determining the arterial transit time of the label between the inversion and the imaging planes. Therefore, a concern with our technique is the variability of arterial transit times between different slices. The graph in Fig. 4 indicates that a 10% error in the measurement of transit time (or a 10% change between measurement of transit time and acquisition of the perfusion time series) translates into a loss (or gain) in signal of up to 15%, depending on whether the transit time is over- or underestimated.

Because of the spread of transit time values (shown in the histogram of Fig. 7), whatever TR is chosen for the turbo-CASL experiment will not be optimal for all voxels in the volume, and there will be a bias in sensitivity toward voxels that have a transit time equal to the chosen TR. The magnitude of this bias will depend on the degree the voxel's transit time differs from the chosen TR (Fig. 4).

At the same time, however, many of the longest times observed in the histogram occur in white-matter voxels, as shown in the transit-time map in Fig. 7 and previously reported in the literature (27). Because of this longer transit time and the lower perfusion rate, white-matter voxels tend to be quite noisy in any ASL-based perfusion measurement, and thus a great deal of the variance is seen in the higher range of transit times. Additionally, white-matter voxels are often disregarded in functional experiments because cognitive activation occurs mostly in the gray matter. It may then be appropriate to bias the measurement toward the gray matter and disregard the low SNR white-matter voxels in the turbo-CASL implementation.

The faster transit times in the histogram likely occurred in areas where the signal was dominated by large arteries. The use of small diffusion-weighting gradients to crush the rapidly arriving arterial signal would effectively eliminate many of the shortest transit times observed in the histogram, and make the measurement more weighted toward microvascular and tissue perfusion.

Quantification can become more difficult if the transit time also varies along the time dimension (i.e., it changes significantly during a period of neuronal activity relative to the resting state). Our data, together with those in Ref. 28, show that transit time is reduced approximately 10% during periods of activation. These changes in transit time and flow that occur during a stimulation experiment introduce a nonlinear relationship between the turbo-CASL signal and the underlying perfusion, as illustrated by Fig. 4. The simulations presented here hold true for steady-state systems (i.e., constant flow and transit time), but in the case of dynamic changes, the ASL signal is likely to represent a distorted version of the underlying flow function. The present theoretical framework approximates the ASL signal, but it would be more appropriate to develop a model that reflects this nonlinear signal behavior. We believe the current models are ill-suited for accurate quantification of perfusion using turbo-CASL because of this technique's sensitivity to variation in transit times, and we are currently developing a more suitable mathematical framework for a dynamically changing system. Nevertheless, our data clearly show that the turbo-CASL approach is very effective in detecting neuronal activation, even in event-related experiments. It should be noted that the activation-induced transit time changes presented here were measured in a block-design motor task, which produces very large changes in BOLD response and thus represents an upper limit of what to expect in a routine fMRI experiment.

Arterial Compartment

Most models developed for quantitative perfusion measurements are geared toward the microvasculature and tissue perfusion. ASL sequences normally employ gradient crushers or delays to suppress the arterial signal contribution in the image.

For functional imaging purposes, however, we have observed that neuronal activation elicits vast changes in the arterial ASL signal (i.e., the ASL signal increases in the absence of arterial suppression are far greater than such increases in the presence of suppression). Thus, we minimized the amount of suppression of arterial flow in order to suppress only the largest arteries with the fastest flow. Additionally, we must consider that turbo-CASL is quite sensitive to changes in transit time. Blood reaches the arteries at the slice of interest earlier than it reaches the tissue bed by approximately 500 ms (Ref. 29 and our own observations), so our data are weighted toward the arterial compartment. We are currently developing a model that contains two separate compartments for the arterial and tissue components.

CONCLUSIONS

We have presented a new approach for obtaining fast CASL measurements of perfusion that is suitable for event-related functional imaging experiments. These measurements are sensitive to changes in transit time, which introduce errors in the quantification of the measurements. From a practical standpoint, however, our data show that turbo-CASL is well suited for detecting perfusion responses in both block-design and event-related experiments.

REFERENCES

1. Mandeville JB, Marota JJA, Kosofsky BE, Keltner JR, Weissleder R, Rosen BR, Weisskoff RM. Dynamic functional imaging of relative cere-

bral volume during rat forepaw stimulation. Magn Reson Med 1998;39: 615–624.
2. Hyder F, Fahmeed, Shulman RG, Rothman DL. A model for the regulation of cerebral oxygen delivery. J Appl Physiol 1998;85:554–564.
3. Vazquez AL, Noll DC. Non-linear aspects of the blood oxygenation response in functional MRI. NeuroImage 1998;7:108–118.
4. Boynton GM, Engel SA, Glover GH, Heeger DJ. Linear systems analysis of functional magnetic resonance imaging in human V1. J Neurosci 1996;16:4207–4221.
5. Friston KJ, Holmes AP, Poline JB, Grasby PJ, Williams SCR, Frackowiak RSJ, Turner R. Analysis of fMRI time series revisited. Neuroimage 1995;2:45–53.
6. Duong TQ, Yacoub E, Adriany G, Hu XP, Ugurbil K, Vaughan JT, Merle H, Kim SG. High-resolution, spin-echo BOLD, CBF fMRI at 4 and 7 T. Magn Reson Med 2002;48:589–593.
7. Pfeuffer J, Adriany G, Shmuel A, Yacoub E, Van der Moorele PF, Hu XP, Ugurbil K. Perfusion-based high-resolution functional imaging in the human brain at 7 Tesla. Magn Reson Med 2002;47:903–911.
8. Williams DS, Detre JA, Leigh JS, Koretsky AP. Magnetic resonance imaging of perfusion using spin inversion of arterial water. Proc Natl Acad Sci USA 1992;89:212–216.
9. Kim SG. Quantification of relative cerebral blood flow change by flow sensitive alternating inversion recovery (FAIR) technique: application to functional mapping. Magn Reson Med 1995;34:293–301.
10. Detre JA, Leigh JS, Williams DS, Koretsky AP. Perfusion imaging. Magn Reson Med 1992;23:37–45.
11. Alsop DC, Detre JA. Reduced transit-time sensitivity in noninvasive magnetic resonance imaging of human cerebral blood flow. J Cereb Blood Flow Metab 1996;16:1236–1249.
12. Purdon PL, Weisskoff RM. Effect of temporal autocorrelation due to physiological noise and stimulus paradigm on voxel-level false-positive rates in fMRI. Hum Brain Mapp 1998;6:239–249.
13. Aguirre GK, Detre JA, Zarahn E, Alsop DC. Experimental design and the relative sensitivity of BOLD and perfusion fMRI. Neuroimage 2002;15: 488–500.
14. Desmond JE, Glover GH. Estimating the sample size in functional MRI (fMRI) neuroimaging studies: statistical power analyses. J Neurosci Methods 2002;118:115–128.
15. Pawlik G, Rackl A, Bing RJ. Quantitative capillary topography and blood flow in the cerebral cortex of cats: an in vivo microscopic study. Brain Res 1981;208:35–58.
16. Weiss HR, Buchweitz E, Murtha TJ, Aluetta M. Quantitative regional determination of the total and perfused capillary network in the rat brain. Circ Res 1982;51:494–503.
17. Silva AC, Zhang W, Williams DS, Koretsky AP. Multi-slice perfusion imaging of the rat brain by arterial spin labeling using two actively decoupled coils. In: Proceedings of the 12th Annual Meeting of SMRM, New York, 1993. p 632.
18. Silva AC, Zhang W, Williams DS, Koretsky AP. Multi-slice MRI of rat brain perfusion during amphetamine stimulation using arterial spin labeling. Magn Reson Med 1995;33:209–214.
19. Wong EC, Luh WM, Liu TT. Turbo ASL: arterial spin labeling with higher SNR and temporal resolution. Magn Reson Med 2000;44:511–515.
20. Buxton RB, Frank LR, Wong EC, et al. A general kinetic model for quantitative perfusion imaging with arterial spin labeling. Magn Reson Med 1998;40:383–396.
21. Ye FQ, Pekar JJ, Jezzard P, Duyn J, Frank JA, McLaughlin AC. Perfusion imaging of the human brain at 1.5T using a single shot EPI spin tagging approach. Magn Reson Med 1996;36:219–224.
22. Lu H, Clingman C, Golay X, van Zijl P. What is the longitudinal relaxation time (T 1) of blood at 3.0 Tesla? In: Proceedings of the 11th Annual Meeting of ISMRM, Toronto, Canada, 2003. p 669.
23. Herscovitch P, Raichle ME. What is the correct value for the brain-blood partition coefficient for water? J Cereb Blood Flow Metab 1985; 1:65–69.
24. Zaharchuk G, Ledden PJ, Kwong KK, Reese TG, Rosen BR, Wald LL. Multi-slice perfusion and perfusion territory imaging in humans with separate label and image coils. Magn Reson Med 1999;41:1093–1098.
25. Lee GR, Hernandez-Garcia L, Noll DC. A phantom for quantitative spin tagging perfusion measurements. In: Proceedings of the 10th Annual Meeting of ISMRM, Honolulu, 2002. p 1057.
26. Jenkinson M, Bannister P, Brady M, Smith S. Improved optimisation for the robust and accurate linear registration and motion correction of brain images. NeuroImage 2002;17:825–841.
27. Ye FQ, Mattay VS, Frank JA, Weinberger DR, McLaughlin AC. Comparison of white and grey matter arterial transit times in spin tagging experiments. In: Proceedings of the 7th Annual Meeting of ISMRM, Philadelphia, 1999. p 1847.
28. Gonzalez JB, Alsop DC, Detre JA. Cerebral perfusion and arterial transit time changes during task activation determined with continuous arterial spin labeling. Magn Reson Med 2000;43:739.
29. Ye FQ, Mattay VS, Jezzard P, Frank JA, Weinberger DR, McLaughlin AC. Correction for vascular artifacts in cerebral blood flow values measured by using arterial spin tagging techniques. Magn Reson Med 1997;37:226–235.